

Time Evolution of an Infinite Projected Entangled Pair State: an Algorithm from First Principles

Piotr Czarnik¹ and Jacek Dziarmaga²

¹*Institute of Nuclear Physics, Polish Academy of Sciences, Radzikowskiego 152, PL-31342 Kraków, Poland*

²*Institute of Physics, Jagiellonian University, Łojasiewicza 11, PL-30348 Kraków, Poland*

(Dated: December 14, 2024)

A quantum state obeying the area law for entanglement on an infinite 2D lattice can be represented by a tensor network ansatz – known as an infinite projected entangled pair state (iPEPS) – with a finite bond dimension D . Its real/imaginary time evolution can be split into small time steps. An application of a time step generates a new iPEPS with a bond dimension k times the original one. The new iPEPS does not make optimal use of its enlarged bond dimension kD , hence in principle it can be represented accurately by a more compact ansatz, favourably with the original D . In this work we show how the more compact iPEPS can be optimized variationally to maximize its overlap with the new iPEPS. The key point is an efficient calculation of the overlap with the corner transfer matrix renormalization group. Using proposed algorithm we provide proof of principle that real time evolution can be simulated by iPEPS simulating sudden quench of the transverse field in 2D quantum Ising model. We test our algorithm in the 2D quantum Ising model by simulating time evolution after a sudden quench of the transverse field. This is a proof of principle demonstration of real time evolution simulation by iPEPS. As similar proof is provided in the same model for imaginary time evolution of purification of its thermal states.

I. INTRODUCTION

Tensor networks are natural language to represent quantum states of strongly correlated systems^{1,12}. Among them the most widely used ansatze are a matrix product states (MPS)² and its 2D generalization: pair-entangled projected state (PEPS)³ also known as a tensor product state. Both obey the area law for entanglement entropy. Matrix product states are efficient parametrizations of ground states of 1D gapped local Hamiltonians^{1,5,6} and purifications of thermal states of 1D local Hamiltonians⁷. MPS is the ansatz optimized by the density matrix renormalization group (DMRG)^{8,9} which is one of the most powerful methods to simulate not only ground states of 1D systems but also their excited states, thermal states or dynamic properties^{10,11}.

The pair-entangled projected states are expected to be an efficient parametrization of ground states of 2D gapped local Hamiltonians^{1,12} and were shown to be an efficient representation of thermal states of 2D local Hamiltonians¹³. Despite huge potential their applications were hindered by technical difficulties¹². Nevertheless, treated as variational ansatze for ground states^{3,4}, recently they became a basis for promising new methods in the field of strongly correlated systems, as demonstrated by solution of a long standing magnetization plateaus problem in highly frustrated compound $\text{SrCu}_2(\text{BO}_3)_2$ ^{14,15} or obtaining coexistence of superconductivity and striped order in the underdoped regime of the Hubbard model – a result which is corroborated by other numerical methods (among them another tensor network approach - DMRG simulations of finite-width cylinders) – apparently settling one of long standing controversies concerning that model¹⁶. Another example of a recent contribution of PEPS-based methods to condensed matter physics is a problem of existence and na-

ture of spin liquid phase in kagome Heisenberg antiferromagnet for which new evidence in support of gapless spin liquid was obtained¹⁷. This progress was accompanied and partly made possible by new developments in PEPS optimization^{18,19}, PEPS contraction^{20–22}, new methods of energy extrapolations²³, and introduction of controlled methods of universality class estimation^{24–26}.

These achievements encourage attempts to use PEPS to simulate thermal states^{22,27–33}, dissipative systems³⁴, many body localization³⁵ or excited states³⁶. Some of those new methods have been already applied to open challenging problems. Those methods attempt to apply PEPS to simulation of broad class of states obeying 2D area law.

Furthermore, there is a lot of theoretical and numerical evidence^{37,38} that PEPS can handle equally well bosonic, spin, or fermionic systems making it applicable beyond the scope of applicability of the well established quantum Monte Carlo methods.

Recent years brought also progress in using DMRG to simulate cylinders with finite width. Such simulations are routinely used alongside iPEPS to investigate 2D systems ground state (see e. g. Ref. 16). These methods have been applied recently also to thermal state simulations^{47,55}.

Among alternative tensor network approaches to strongly correlated systems are methods of direct contraction and renormalization of a 3D tensor network representing a density operator of a 2D thermal state^{48–54} and technically challenging yet able to represent breaking area law 1D critical states Multi-Scale Entanglement Renormalization Ansatz (MERA) ansatz⁵⁹.

In this work we propose an algorithm to simulate either real or imaginary time evolution with infinite PEPS. The algorithm uses Suzuki-Trotter decomposition of the evolution operator into small time steps. A straightforward

application of a time step creates a new iPEPS with a bond dimension k times the original bond dimension D . If not truncated, the evolution would result in an exponential growth of the bond dimension. We propose a variational scheme where the new iPEPS is approximated variationally by an iPEPS with the original D . The key element of the algorithm is evaluation of an overlap between the new iPEPS and its variational approximation by the corner transfer matrix renormalization group^{38–40}.

A challenging application of our method is real time evolution after a sudden quench. A sudden quench of a parameter in a Hamiltonian excites entangled pairs of quasiparticles with opposite quasimomenta that run away from each other crossing the boundary of the subsystem. Consequently, the number of pairs that are entangled across the boundary (proportional to the entanglement entropy) grows linearly with time requiring an exponential growth of the bond dimension. Therefore, a tensor network is doomed to fail after a finite evolution time. Nevertheless, matrix product states proved to be useful for simulating time evolution after sudden quenches in 1D⁴¹. As a proof of principle that the same can be done with iPEPS in 2D, in this work we simulate a sudden quench in the transverse field quantum Ising model.

Moreover, there are other – easier from the entanglement point of view – potential applications of the real time variational evolution. For instance, a smooth ramp of a parameter in a Hamiltonian across a quantum critical point generates the entanglement entropy proportional to the area of the boundary times a logarithm of the Kibble-Zurek correlation length $\hat{\xi}$ that in turn is a power of the ramp time⁴². Thanks to this dynamical area law, the required D is not an exponential but a mere power of the ramp time. Even stronger limitations may apply in many-body localization, where localized excitations are not able to spread the entanglement. Finally, with a straightforward vectorization of the density matrix, the unitary time evolution can be generalized to a Markovian master equation with a Lindblad superoperator, where local decoherence limits the entanglement making the time evolution with a tensor network feasible³⁴.

Another promising application is imaginary time evolution generating thermal states of a quantum Hamiltonian. By definition, a thermal Gibbs state maximizes entropy for a given average energy. As this maximal entropy is the entropy of entanglement of the system with the rest of the universe, then – by the monogamy of entanglement – there is little entanglement left inside the system. In more quantitative terms, both thermal states of local Hamiltonians and PEPS representations of density operators obey area law for mutual information making an iPEPS a good ansatz for thermal states⁴³. In this paper we evolve a purification of thermal states in the quantum Ising model obtaining results convergent to the variational tensor network renormalization (VTNR) introduced and applied to a number of models in^{22,30–32}. This test is a proof of principle that thermal states can

be obtained with the proposed variational imaginary time evolution.

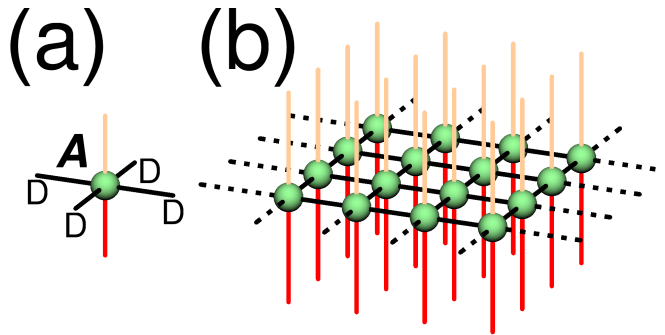


FIG. 1. In a, an elementary rank-6 tensor A of a purification. The top (orange) index numbers ancilla states $a = 0, 1$, the bottom (red) index numbers spins states $s = 0, 1$, the four (black) bond indices have a bond dimension D . In b, a PEPS representation of the purification. Here pairs of elementary tensors at NN lattice sites were contracted through their connecting bond indices. The whole network is an amplitude for a joint spins and ancillas state labelled by the open spin and ancilla indices. Reducing the dimension of ancilla indices to 1 (or simply ignoring the ancilla lines) we obtain a well known PEPS representation of a pure state.

The paper is organized as follows. In section II we briefly introduce the quantum Ising model in a transverse field. In section III we introduce purification of a thermal state to be evolved in imaginary time. In section IV we introduce the algorithm in the more general case of imaginary time evolution of a thermal state purification. A modification/reduction to real time evolution of a pure state is straightforward. In subsection IV A we make Suzuki-Trotter decomposition of a small time step and represent it by a tensor network. In subsection IV B we outline the general idea of the algorithm. Further details are refined in subsections IV C, IV D, and appendix A.

In section V the algorithm is applied to simulate imaginary time evolution generating thermal states. Obtained results are compared with VTNR. In section VI the real time version of the algorithm is tested in the challenging problem of time evolution after a sudden quench.

Finally, we conclude in section VII.

II. QUANTUM ISING MODEL

We will exemplify the general idea with the transverse field quantum Ising model on an infinite square lattice

$$H = - \sum_{\langle j, j' \rangle} Z_j Z_{j'} - \sum_j (h_x X_j + h_z Z_j). \quad (1)$$

Here Z, X are Pauli matrices. At zero longitudinal bias, $h_z = 0$, the model has a ferromagnetic phase with a non-zero spontaneous magnetization $\langle Z \rangle$ for sufficiently small

transverse field h_x and sufficiently large inverse temperature β . At $h_x = 0$ the critical β is $\beta_0 = -\ln(\sqrt{2}-1)/2 \approx 0.441$ and at zero temperature the quantum critical point is $h_0 = 3.04438(2)$, see Ref. 44.

III. PURIFICATION OF THERMAL STATES

In an enlarged Hilbert space, every spin with states $s = 0, 1$ is accompanied by an ancilla with states $a = 0, 1$. The space is spanned by states $\prod_j |s_j, a_j\rangle$, where j is a lattice site. The Gibbs operator at an inverse temperature β is obtained from its purification $|\psi(\beta)\rangle$ (defined in the enlarged space) by tracing out the ancillas,

$$\rho(\beta) \propto e^{-\beta H} = \text{Tr}_{\text{ancillas}} |\psi(\beta)\rangle \langle \psi(\beta)|. \quad (2)$$

At $\beta = 0$ we choose a product over lattice sites,

$$|\psi(0)\rangle = \prod_j \sum_{s=0,1} |s_j, s_j\rangle, \quad (3)$$

to initialize the imaginary time evolution

$$|\psi(\beta)\rangle = e^{-\frac{1}{2}\beta H} |\psi(0)\rangle = U(-i\beta/2) |\psi(0)\rangle. \quad (4)$$

The evolution operator $U(\tau) = e^{-i\tau H}$ acts in the Hilbert space of spins. With the initial state (3) Eq. (2) becomes

$$\rho(\beta) \propto U(-i\beta/2) U^\dagger(-i\beta/2). \quad (5)$$

Just like a pure state of spins, the purification can be represented by a PEPS, see Fig. 1.

IV. THE METHOD

We introduce the algorithm in the more general case of thermal states simulation by imaginary time evolution of their purification. To be more specific, we use the example of the quantum Ising model. Generalization to other models is as straightforward as a modification to real time evolution. The latter one amounts to ignoring any ancilla lines in the diagrams.

A. Suzuki-Trotter decomposition

In the second-order Suzuki-Trotter decomposition a small time step is

$$U(d\tau) = U_h(d\tau/2) U_{ZZ}(d\tau) U_h(d\tau/2), \quad (6)$$

where

$$U_{ZZ}(d\tau) = \prod_{\langle j,j'\rangle} e^{id\tau Z_j Z_{j'}}, \quad U_h(d\tau) = \prod_j e^{id\tau h_j} \quad (7)$$

are elementary gates and $h_j = h_x X_j + h_z Z_j$.

In order to rearrange $U(d\tau)$ as a tensor network, we use singular value decomposition to rewrite a 2-site term

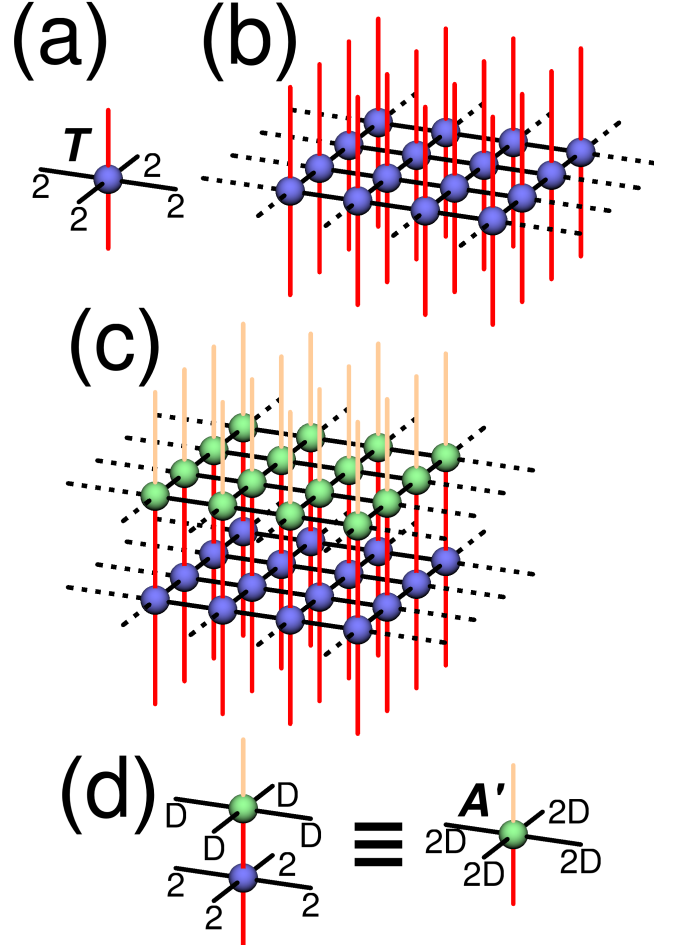


FIG. 2. In a, an elementary rank-6 Trotter tensor T with two (red) spin indices and four (black) bond indices, each of dimension 2. In b, a layer of Trotter tensors representing a small time step $U(d\tau)$. In c, the time step $U(d\tau)$ is applied to spin indices of the purification. In d, the tensors T and A can be contracted into a single new tensor A' . A layer of A' makes a new PEPS that looks like the original one in Fig. 1b but has a doubled bond dimension $2D$.

$e^{id\tau Z_j Z_{j'}}$ acting on a NN bond as a contraction of 2 smaller tensors acting on single sites:

$$e^{id\tau Z_j Z_{j'}} = \sum_{\mu=0,1} z_{j,\mu} z_{j',\mu}. \quad (8)$$

Here μ is a bond index and $z_{j,\mu} \equiv \sqrt{\Lambda_\mu} (Z_j)^\mu$ and $\Lambda_0 = \cos d\tau$ and $\Lambda_1 = i \sin d\tau$. Now we can write

$$U(d\tau) = \sum_{\{\mu\}} \prod_j \left[e^{id\tau h_j/2} \left(\prod_{j'} z_{j,\mu_{\langle j,j'\rangle}} \right) e^{id\tau h_j/2} \right]. \quad (9)$$

Here $\mu_{\langle j,j'\rangle}$ is a bond index on the NN bond $\langle j,j'\rangle$ and $\{\mu\}$ is a collection of all such bond indices. The square brackets enclose a Trotter tensor $T(d\tau)$ at site j , see Fig. 2a. It is a spin operator depending on the bond

indices connecting its site with its four NNs. A contraction of these Trotter tensors is the gate $U(d\tau)$ in Fig. 2b. The evolution operator is a product of such time steps, $U(Nd\tau) = [U(d\tau)]^N$.

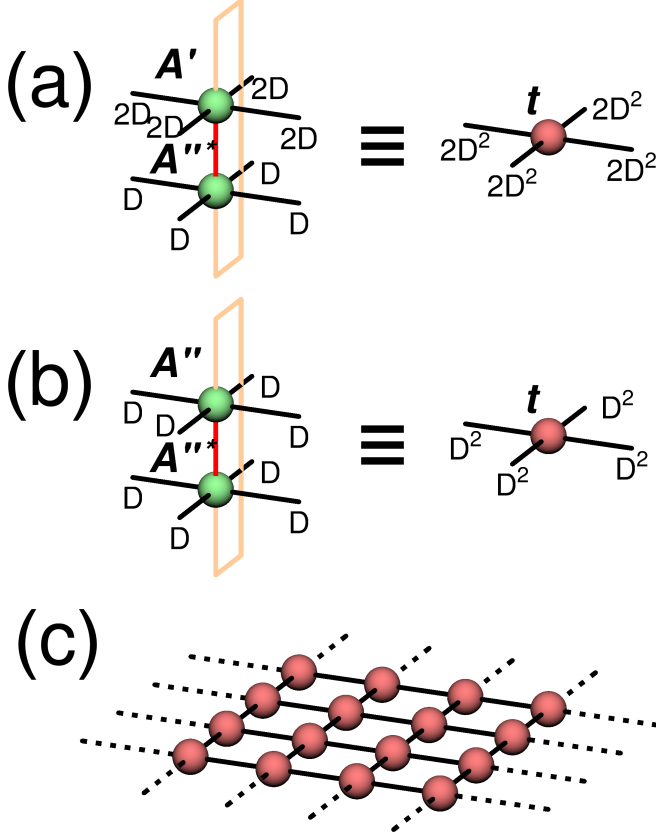


FIG. 3. In a, tensor A' is contracted with a complex conjugate of A'' into a transfer tensor t with a bond dimension $d = 2D^2$. In b, tensor A'' is contracted with its own complex conjugate into a transfer tensor t with a bond dimension $d = D^2$. In c, an infinite layer of tensors t – defined in (a) and (b) – represents the overlap $\langle \psi'' | \psi' \rangle$ or $\langle \psi'' | \psi'' \rangle$, respectively.

B. Variational truncation

The time step $U(d\tau)$ applied to the state $|\psi\rangle$ yields a new state

$$|\psi'\rangle = U(d\tau)|\psi\rangle, \quad (10)$$

see Figs. 2c and d. If $|\psi\rangle$ has a bond dimension D , then the new PEPS has twice the original bond dimension $2D$.

In order to prevent exponential growth of the dimension in time, the new PEPS has to be approximated by a more compact one, $|\psi''\rangle$, made of tensors A'' with the original bond dimension D . The best $|\psi''\rangle$ minimizes the norm

$$\| |\psi''\rangle - |\psi'\rangle \|^2. \quad (11)$$

Equivalently – up to normalization of $|\psi''\rangle$ – the quality of the approximation can be measured by a global fidelity

$$F = \frac{\langle \psi'' | \psi' \rangle \langle \psi' | \psi'' \rangle}{\langle \psi'' | \psi'' \rangle}. \quad (12)$$

After a rearrangement in section IV C below, it becomes an efficient figure of merit.

The PEPS tensor A'' – the same at all sites – has to be optimized globally. However, the first step towards this global optimum is a local pre-update. We choose a site j and label the tensor at this site as A''_j . This tensor is optimized while all other tensors are kept fixed as A'' . With the last constraint the norm (11) becomes a quadratic form in A''_j . The quadratic form is minimized with respect to A''_j by

$$\tilde{A} = G^{-1}V. \quad (13)$$

Here

$$G = \frac{\partial^2 \langle \psi'' | \psi'' \rangle}{\partial (A''_j)^* \partial (A''_j)}, \quad V = \frac{\partial \langle \psi'' | \psi' \rangle}{\partial (A''_j)^*} \quad (14)$$

are, respectively, a metric tensor and a gradient. Further details on the local pre-update can be found in section IV D below.

The global fidelity (12) is not warranted to increase when the local optimum \tilde{A} is substituted globally, i.e., in place of every A'' at every lattice site. However, \tilde{A} can be used as an estimate of the most desired direction of the change of A'' . In this vein, we attempt an update

$$A'' = A \cos \epsilon + \tilde{A} \sin \epsilon, \quad (15)$$

with an adjustable parameter $\epsilon \in [-\pi/2, \pi/2]$ using an algorithm proposed in Ref. 18⁵⁷. This update was successfully used in a similar variational problem of minimizing energy of infinite PEPS as a function of A ¹⁸. We see that it leads to systematic improvement of the overlap in our case. Once A'' in (15) is accepted, the whole procedure beginning with (13) is iterated until F is converged. The converged A'' is accepted as a global optimum.

C. Efficient overlap computation

In the limit of infinite lattice, the overlaps in the fidelity (12) become

$$\langle \psi'' | \psi' \rangle = \lim_{N \rightarrow \infty} n^N, \quad \langle \psi'' | \psi'' \rangle = \lim_{N \rightarrow \infty} d^N, \quad (16)$$

where N is the number of lattice sites. Consequently, the fidelity becomes $F = \lim_{N \rightarrow \infty} f^N$, where

$$f = \frac{nn^*}{d} \quad (17)$$

is a figure of merit per site.

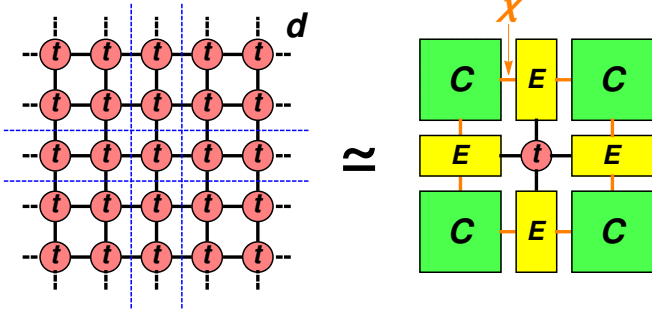


FIG. 4. Left, planar version of Fig. 3c. Right, its approximate representation with corner tensors C and edge tensors E . Here C effectively represents a corner of the infinite graph on the left and E its semi-infinite edge. Environmental bond dimension χ controls accuracy of the approximation. Tensors C and E are obtained with corner transfer matrix renormalization group^{38–40}.

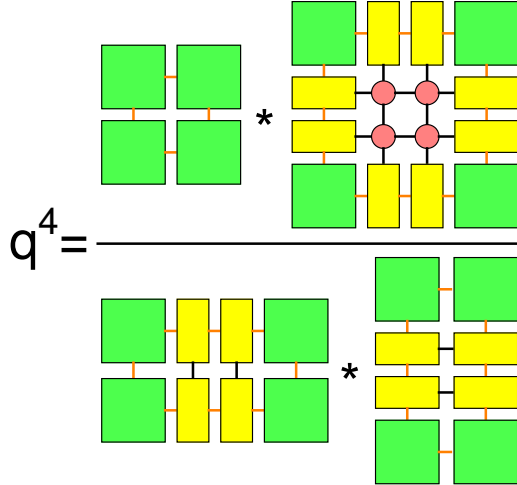


FIG. 5. The environmental tensors introduced in Fig. 4 can be used to calculate the figure of merit (17). This diagram shows a factor q^4 by which the diagram in Fig. 3c (or, equivalently, the left panel of Fig. 4) is multiplied when 4 site is added to the network. Depending on the overlap in question – either $\langle \psi'' | \psi' \rangle$ or $\langle \psi'' | \psi'' \rangle$, see Fig. 3 – the quotient is either $n = q$ or $d = q$, respectively.

The factors n and d can be obtained by a generalization of ideas that can be traced back to Baxter^{39,56}. First of all, each overlap – $\langle \psi'' | \psi' \rangle$ and $\langle \psi'' | \psi'' \rangle$ – can be represented by a planar network in Fig. 3c. With the help of the corner transfer matrix renormalization group (CTMRG)^{38–40}, this infinite network can be effectively replaced by a finite one, as shown in Fig. 4. Figure 5 shows how to obtain n and d with the effective environmental tensors introduced in Fig. 4.

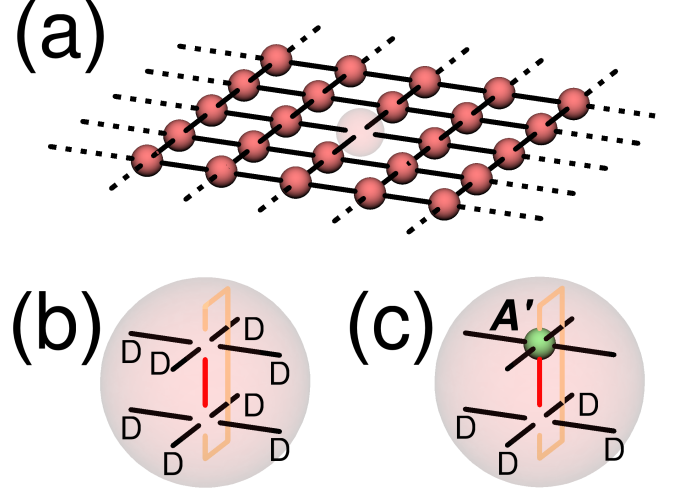


FIG. 6. In a, tensor environment for t . It is obtained by removing one tensor t from the overlap in Fig. 3c or, equivalently, the tensor t from the right diagram in Fig. 4. The environment represents a derivative of the overlap with respect to t in either (18) or (19). This rank-4 tensor has 4 indices with dimension equal to either $D \times D$ or $D \times 2D$, respectively. In b, in case of (18) each of the 4 indices in (a) is decomposed back into two indices, each of dimension D . The diagram represents the metric tensor G . The open (red) spin line is a Kronecker delta for spin states and the open (orange) ancilla line is a delta for ancillas. Therefore, the metric can be decomposed as $G = g \otimes 1_s \otimes 1_a$, where g is the tensor environment for t and 1_s and 1_a are identities for spins and ancillas, respectively. In c, in case of (19) each of the 4 indices in (a) is decomposed back into two indices of dimension $2D$ (upper) and D (lower). After contracting the upper indices with A' the diagram becomes the gradient V .

D. Local pre-update

To construct G and V from CTMRG tensors C, T we rewrite Eq. (14) as

$$G = \frac{\partial \langle \psi'' | \psi'' \rangle}{\partial t} \frac{\partial^2 t}{\partial (A_j'')^* \partial (A_j'')}, \quad (18)$$

$$V = \frac{\partial \langle \psi'' | \psi' \rangle}{\partial t} \frac{\partial t}{\partial (A_j'')^*} \quad (19)$$

The above derivatives of an overlap – either $\langle \psi'' | \psi'' \rangle$ or $\langle \psi'' | \psi' \rangle$ – with respect to t are represented by Fig. 6a, where one tensor t was removed from the overlap shown in Figs. 3c, 4. This rank-4 tensor is a tensor environment for t . Its 4 indices have a dimension equal to either $D \times D$ or $2D \times D$, respectively. This environment can be used to calculate either G or V , as shown in Figs. 6b,c.

Figure 6b demonstrates that the metric G has a tensor-product structure $G = g \otimes 1_s \otimes 1_a$, where g is the tensor environment for t and 1_s and 1_a are identities for spins and ancillas, respectively. Therefore – after proper reshaping of tensors – Eq. (13) simplifies to

$$\tilde{A} = g^{-1}V. \quad (20)$$

Only the small tensor environment g has to be inverted. In this work we use the Moore-Penrose pseudoinverse to treat its null space.

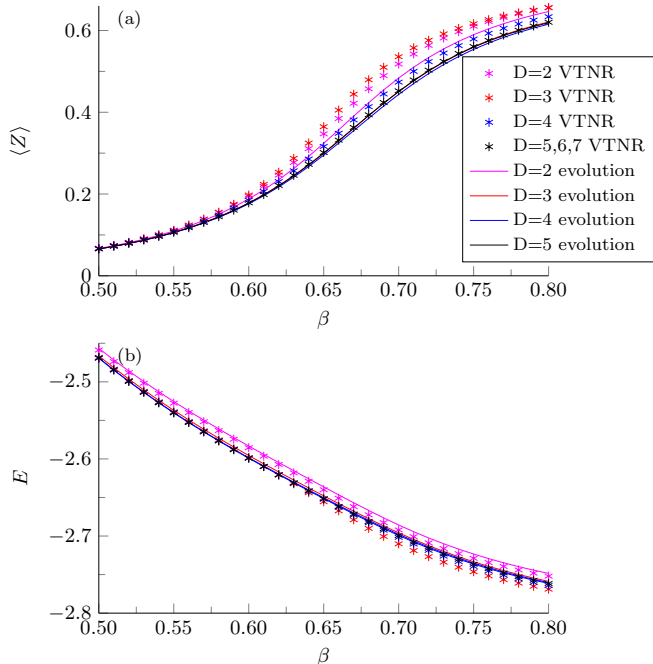


FIG. 7. Thermal states for a transverse field $h_x = 2.5$ with a longitudinal bias $h_z = 0.01$. The stars are results from variational tensor network renormalization (VTNR) and the solid lines from the imaginary time evolution. With increasing bond dimension D the two methods converge to each other. In a, longitudinal magnetization $\langle Z \rangle$ in function of inverse temperature. In b, energy per site E in function of inverse temperature.

V. THERMAL STATES FROM IMAGINARY TIME EVOLUTION

In this section we present results obtained by imaginary time evolution for two values of the transverse field, $h_x = 2.5$ and $h_x = 2.9$, corresponding to critical temperatures $\beta_c = 0.7851(4)$ and $\beta_c = 1.643(2)$, respectively⁴⁵. We show data with $D = 2, 3, 4, 5$. The stronger field is closer to the quantum critical h_0 , hence quantum fluctuations are stronger and bigger bond dimension D is required. For the imaginary time evolution to run smoothly across the critical point we added a small longitudinal bias $h_z = 0.01$.

Figures 7a and 7b show the longitudinal magnetization $\langle Z \rangle$ and energy E for the two transverse fields. The data from the imaginary time evolution are compared to results obtained with the variational tensor network renormalization (VTNR)^{22,30–32}. With increasing D each of the two methods converges and they converge to each other.

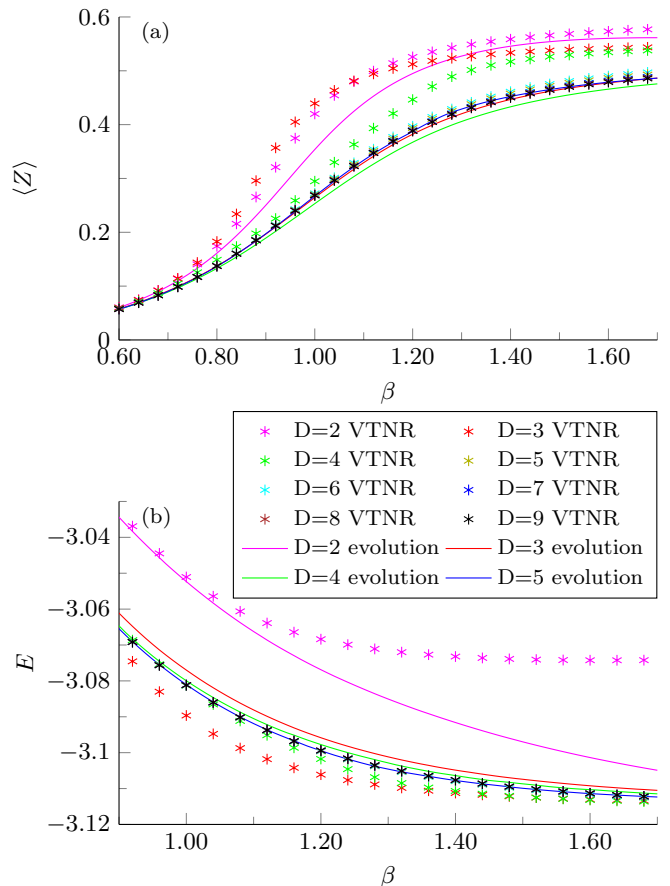


FIG. 8. Thermal states for a transverse field $h_x = 2.9$ with a longitudinal bias $h_z = 0.01$. The stars are results from variational tensor network renormalization (VTNR) and the solid lines from the imaginary time evolution. With increasing bond dimension D the two methods converge to each other. In a, longitudinal magnetization $\langle Z \rangle$ in function of inverse temperature. In b, energy per site E in function of inverse temperature.

This data are proof of principle of applicability of the new method to thermal state simulation.

VI. TIME EVOLUTION AFTER A SUDDEN QUENCH

Next we move to simulation of a real time evolution after a quench in an unbiased model (1) with $h_z = 0$. The initial state is the ground state for $h_x \gg h_0$ with all spins pointing along x . At $t = 0$ the Hamiltonian is suddenly quenched down to a finite $h_x = 2h_0, h_0, h_0/10$ that is, respectively, above, at, and below the quantum critical point h_0 .

Figure 9 shows a time evolution of the magnetization $\langle X \rangle$ and energy per site E after the sudden quench for bond dimensions $D = 2, 3, 4$. With increasing D the energy becomes conserved more accurately for a longer

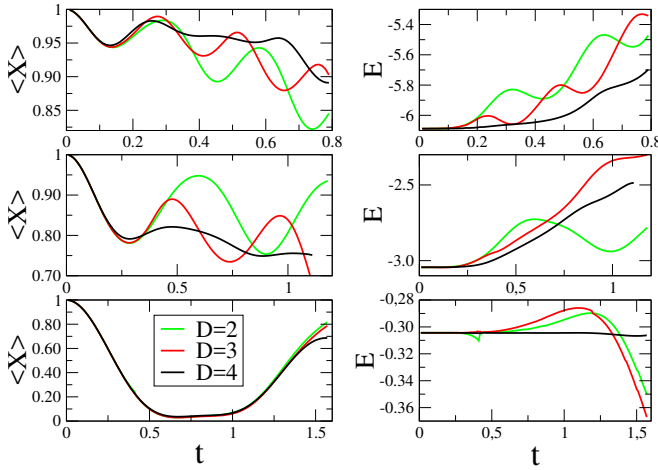


FIG. 9. Transverse magnetization $\langle X \rangle$ (left column) and energy per site (right column) after a sudden quench from a ground state in a strong transverse field, $h_x \gg h_0$, with all spins pointing along x down to a finite $h_x = 2h_0$ (top row), $h_x = h_0$ (middle row), and $h_x = h_0/10$ (bottom row). Energy conservation shows systematic improvement with increasing bond dimension $D = 2, 3, 4$. We see that for sufficiently small times seemingly converged results for transverse magnetization can be obtained. While approaching the limit of small entanglement ($h_x = h_0/10$) we see that the "convergence time" is growing longer as expected.

time. This is an indication of the general convergence of the algorithm.

Not quite surprisingly, the results are most accurate for $h_x = h_0/10$. This weak transverse field is close to $h_x = 0$ when the Hamiltonian is classical and the time evolution can be represented exactly with $D = 2$. At $h_x = 0$ quasiparticles have flat dispersion relation and do not propagate, hence – even though they are excited as entangled pairs with opposite quasi-momenta – they do not spread entanglement across the system. For any $h_x > 0$, however, the entanglement grows with time and any bond dimension is bound to become insufficient after a finite evolution time. However, as discussed in Sec. I, there are many interesting potential applications where this effect is of limited importance.

VII. CONCLUSION

We proposed and tested a straightforward algorithm to simulate real and imaginary time evolution with infinite PEPS. The algorithm is based on variational maximization of an overlap between a new PEPS obtained after direct application of a time step and its approximation by a PEPS with the original bond dimension. The key element is evaluation of the overlap with the corner transfer matrix renormalization group (CTMRG).

The main result is simulation of real time evolution after a sudden quench of a Hamiltonian. With increasing

bond dimension the results converge over increasing evolution time. This is a proof of principle demonstration that simulation of a real time evolution with a 2D tensor network is feasible.

We also apply the same algorithm to evolve purification of thermal states. These results converge to the established VTNR method providing a proof of principle that the new algorithm can be applied to 2D strongly correlated systems at finite temperature.

ACKNOWLEDGMENTS

P. C. acknowledges inspiring discussions with Philippe Corboz on application of CTMRG to calculation of partition function per site and simulations of thermal states. We thank Stefan Wessel for numerical values of data published in Ref. 45. Simulations were done with extensive use of ncon function⁴⁶. This research was funded by National Science Center, Poland under project 2016/23/B/ST3/00830 (PC) and QuantERA program 2017/25/Z/ST2/03028 (JD).

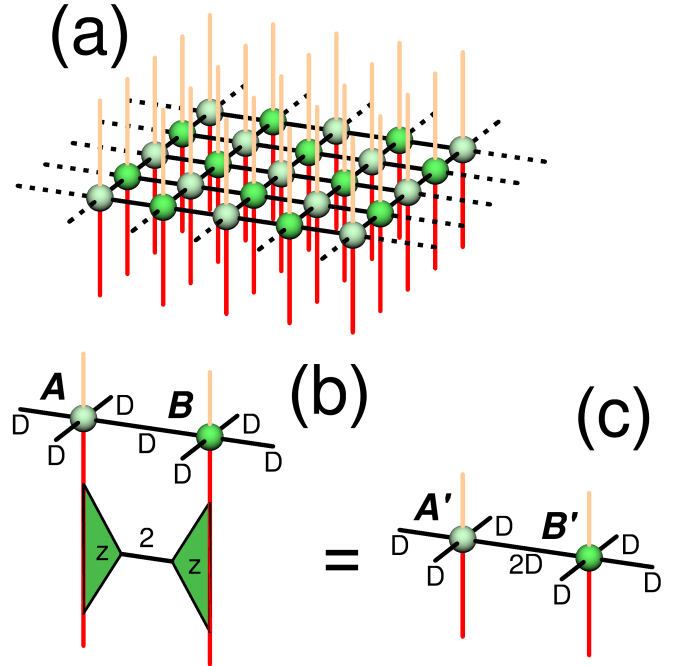


FIG. 10. In a, the infinite square lattice is divided into two sublattices with tensors A (lighter green) and B (darker green). In b, SVD decomposition of a NN gate is applied to every pair A and B of NN tensors. In c, when the tensors A and B are contracted with their respective z 's, then they become new tensors A' and B' with a doubled bond dimension $2D$ on their common NN bond. By variational optimization the PEPS made of A' and B' is approximated by a new PEPS made of A'' and B'' with the original bond dimension D .

Appendix A: 2-site gates

For the sake of clarity, the main text presents a straightforward single-site version of the algorithm. In practice it is more efficient to implement the gate $U_{ZZ}(d\tau)$ as a product of two-site gates. To this end the infinite square lattice is divided into two sublattices A and B , see Fig. 10a. On the checkerboard the gate becomes a product

$$U_{ZZ}(d\tau) = U_0^a(d\tau)U_1^a(d\tau)U_0^b(d\tau)U_1^b(d\tau). \quad (\text{A1})$$

Here a and b are the Cartesian lattice directions spanned by e_a and e_b ,

$$U_s^a(d\tau) = \prod_{mn} e^{id\tau Z_{2m+s-1,n} Z_{2m+s,n}}, \quad (\text{A2})$$

$$U_s^b(d\tau) = \prod_{mn} e^{id\tau Z_{m,2n+s-1} Z_{m,2n+s}}, \quad (\text{A3})$$

and $Z_{m,n}$ is an operator at a site $me_a + ne_b$.

Every NN gate in (A2,A3) is decomposed as in (8). Consequently, when a gate, say, $U_0^a(d\tau)$ is applied to the checkerboard AB -PEPS in Fig. 10a, then every pair of tensors A and B at every pair of NN sites $(2m-1)e_a + ne_b$ and $2me_a + ne_b$ is applied with the NN-gate's decomposition as in Fig. 10b. When the tensors A and B are fused with their respective z 's, they become A' and B' , respectively, that are connected by an index with a bond dimension $2D$, see Fig. 10c. The action of the gate $U_0^a(d\tau)$ is completed when the $A'B'$ -PEPS is approximated by a (variationally optimized) new $A''B''$ -PEPS with the original bond dimension D at every bond.

Apart from the opportunity to use reduced tensors in the variational optimization, the main advantage of the 2-site gates is that the enlarged bond dimension $2D$ appears only on a minority of bonds. This speeds up the CTMRG for the overlap $\langle\psi'|\psi''\rangle$ that is the most time-consuming part of the algorithm.

-
- ¹ F. Verstraete, V. Murg and J.I. Cirac, Adv. in Phys. **58**, 143 (2008).
 - ² M. Fannes, B. Nachtergaele, and R. F. Werner, Communications in Mathematical Physics **144**, 443 (1992).
 - ³ F. Verstraete and J. I. Cirac, cond-mat/0407066 (2004).
 - ⁴ V. Murg, F. Verstraete, and J. I. Cirac, Phys. Rev. A **75**, 033605 (2007); Y. Nishio, N. Maeshima, A. Gendiar, and T. Nishino, cond-mat/0401115 (2004); Z.-C. Gu, M. Levin, and X.-G. Wen, Phys. Rev. B **78**, 205116 (2008); J. Jordan, R. Orús, G. Vidal, F. Verstraete, and J. I. Cirac, Phys. Rev. Lett. **101**, 250602 (2008); H. C. Jiang, Z. Y. Weng, and T. Xiang, *ibid.* **101**, 090603 (2008); Z. Y. Xie, H. C. Jiang, Q. N. Chen, Z. Y. Weng, and T. Xiang, *ibid.* **103**, 160601 (2009); P.-C. Chen, C.-Y. Lai, and M.-F. Yang, J. Stat. Mech.: Theory Exp. (2009) P10001;
 - ⁵ M.B. Hastings, J. Stat. Phys. **8** (2007), P08024.
 - ⁶ N. Schuch, M.M. Wolf, F. Verstraete and J.I. Cirac, Phys. Rev. Lett. **100** (2008), 030504.
 - ⁷ T. Barthel, arXiv:1708.09349, (2017).
 - ⁸ S. R. White, Phys. Rev. Lett. **69**, 2863 (1992).
 - ⁹ S. R. White, S. R. White, Phys. Rev. B **48**, 10345 (1993).
 - ¹⁰ U. Schollwöck, Rev. Mod. Phys. **77**, 259 (2005).
 - ¹¹ U. Schollwöck, Annals of Physics **326**, 96 (2011).
 - ¹² R. Orús, Ann. of Phys. **349**, 117 (2014).
 - ¹³ A. Molnár, N. Schuch, F. Verstraete, and J. I. Cirac, Phys. Rev. B **91**, 045138 (2015).
 - ¹⁴ Y. H. Matsuda, N. Abe, S. Takeyama, H. Kageyama, P. Corboz, A. Honecker, S. R. Manmana, G. R. Foltin, K. P. Schmidt, and F. Mila, Phys. Rev. Lett. **111**, 137204 (2013).
 - ¹⁵ P. Corboz, and F. Mila, Phys. Rev. Lett. **112**, 147203 (2014).
 - ¹⁶ B.-X. Zheng, C.-M. Chung, P. Corboz, G. Ehlers, M.-P. Qin, R. M. Noack, H. Shi, S. R. White, S. Zhang, and G. K.-L. Chan, Science **358**, 1155 (2017).
 - ¹⁷ H. J. Liao, Z. Y. Xie, J. Chen, Z. Y. Liu, H. D. Xie, R. Z. Huang, B. Normand, and T. Xiang, Phys. Rev. Lett. **118**, 137202 (2017).
 - ¹⁸ P. Corboz, Phys. Rev. B **94**, 035133 (2016).
 - ¹⁹ L. Vanderstraeten, J. Haegeman, P. Corboz, and F. Verstraete, Phys. Rev. B **94**, 155123 (2016).
 - ²⁰ M.T. Fishman, L. Vanderstraeten, V. Zauner-Stauber, J. Haegeman, and F. Verstraete, arXiv:1711.05881.
 - ²¹ Z. Y. Xie, H. J. Liao, R. Z. Huang, H. D. Xie, J. Chen, Z. Y. Liu, and T. Xiang, Phys. Rev. B **96**, 045128 (2017).
 - ²² P. Czarnik, M. M. Rams, and J. Dziarmaga, Phys. Rev. B **94**, 235142 (2016).
 - ²³ P. Corboz, Phys. Rev. B **93**, 045116 (2016).
 - ²⁴ P. Corboz, P. Czarnik, G. Kapetijns, and L. Tagliacozzo, arXiv:1803.08445.
 - ²⁵ M. Rader, and A. M. Läuchli, arXiv:1803.08566.
 - ²⁶ M. M. Rams, P. Czarnik, and L. Cincio, arXiv:1801.08554.
 - ²⁷ P. Czarnik, L. Cincio, and J. Dziarmaga, Phys. Rev. B **86**, 245101 (2012).
 - ²⁸ P. Czarnik and J. Dziarmaga, Phys. Rev. B **90**, 035144 (2014).
 - ²⁹ P. Czarnik, and J. Dziarmaga, Phys. Rev. B **92**, 035120 (2015).
 - ³⁰ P. Czarnik and J. Dziarmaga, Phys. Rev. B **92**, 035152 (2015).
 - ³¹ P. Czarnik, J. Dziarmaga, and A. M. Oleś, Phys. Rev. B **93**, 184410 (2016).
 - ³² P. Czarnik, J. Dziarmaga, and A. M. Oleś, Phys. Rev. B **96**, 014420 (2017).
 - ³³ Y.-W. Dai, Q.-Q. Shi, S. Y. Cho, M. T. Batchelor, and H.-Q. Zhou, Phys. Rev. B **95**, 214409 (2017).
 - ³⁴ A. Kshetrimayum, H. Weimer, and R. Orús, Nature Communications **8**, 1291 (2017);
 - ³⁵ T. B. Wahl, A. Pal, and S. H. Simon, arXiv:1711.02678;
 - ³⁶ L. Vanderstraeten, M. Mariën, F. Verstraete, and J. Haegeman, Phys. Rev. B **92**, 201111 (2015).
 - ³⁷ T. Barthel, C. Pineda, and J. Eisert, Phys. Rev. A **80**, 042333 (2009); P. Corboz and G. Vidal, Phys. Rev. B **80**, 165129 (2009); P. Corboz, G. Evenbly, F. Verstraete, and G. Vidal, Phys. Rev. A **81**, 010303(R) (2010); C. V. Kraus, N. Schuch, F. Verstraete, and J. I. Cirac, *ibid.* **81**, 052338 (2010); C. Pineda, T. Barthel, and J. Eisert, *ibid.* **81**, 050303(R) (2010); Z.-C. Gu, F. Verstraete, and X.-G. Wen,

- arXiv:1004.2563 (2010). P. Corboz, R. Orús, B. Bauer, and G. Vidal, Phys. Rev. B **81**, 165104 (2010); P. Corboz, S. R. White, G. Vidal, and M. Troyer, *ibid.* **84**, 041108 (2011).
- ³⁸ P. Corboz, T. M. Rice, and M. Troyer, Phys. Rev. Lett. **113**, 046402 (2014).
- ³⁹ R. J. Baxter, J. Stat. Phys. **19**, 461 (1978);
- ⁴⁰ T. Nishino and K. Okunishi, J. Phys. Soc. Jpn. **65**, 891 (1996); R. Orús and G. Vidal, Phys. Rev. B **80**, 094403 (2009);
- ⁴¹ J. C. Halimeh and V. Zauner-Stauber, Phys. Rev. B **96**, 134427 (2017).
- ⁴² L. Cincio, J. Dziarmaga, M. M. Rams, W. H. Zurek, Phys. Rev. A **75**, 052321 (2007).
- ⁴³ M.M. Wolf, F. Verstraete, M.B. Hastings, and J.I. Cirac, Phys. Rev. Lett. **100**, 070502 (2008).
- ⁴⁴ H. W. J. Blote and Y. Deng, Phys. Rev. E **66**, 066110 (2002).
- ⁴⁵ S. Hesselmann, and S. Wessel, Phys. Rev. B **93**, 155157 (2016).
- ⁴⁶ R. N. C. Pfeifer, G. Evenbly, S. Singh, and G. Vidal, arXiv:1402.0939 (2014).
- ⁴⁷ B. Bruognolo, Z. Zhu, S. R. White, and E. M. Stoudenmire, arXiv:1705.05578.
- ⁴⁸ W. Li, S.-J. Ran, S.-S. Gong, Y. Zhao, B. Xi, F. Ye, and G. Su, Phys. Rev. Lett. **106**, 127202 (2011).
- ⁴⁹ Z. Y. Xie, J. Chen, M. P. Qin, J. W. Zhu, L. P. Yang, and T. Xiang, Phys. Rev. B **86**, 045139 (2012).
- ⁵⁰ Shi-Ju Ran, Wei Li, Bin Xi, Zhe Zhang, and Gang Su, Phys. Rev. B **86**, 134429 (2012).
- ⁵¹ S.-J. Ran, B. Xi, T. Liu, and G. Su, Phys. Rev. B **88**, 064407 (2013).
- ⁵² S.-J. Ran, W. Li, S.-S. Gong, A. Weichselbaum, J. von Delft, and G. Su, Phys. Rev. B **97**, 075146 (2018).
- ⁵³ C. Peng, S.-J. Ran, T. Liu, X. Chen, and G. Su, Phys. Rev. B **95**, 075140 (2017).
- ⁵⁴ X. Chen, S.-J. Ran, T. Liu, C. Peng, Y.-Z. Huang, and G. Su, arXiv:1711.01001.
- ⁵⁵ B.-B. Chen, L. Chen, Z. Chen, W. Li, and A. Weichselbaum, arXiv:1801.00142.
- ⁵⁶ R. J. Baxter, and I. G. Enting, J. Stat. Phys., **21**, 103, (1979); Chan, Y., J. Phys. A: Math. Theor. **45**, 085001, (2012); Chan, Y., J. Phys. A: Math. Theor. **46**, 125009, (2013).
- ⁵⁷ Its less advanced version was introduced in Ref. 58.
- ⁵⁸ T. Nishino, Y. Hieida, K. Okunishi, N. Maeshima, Y. Akutsu, and A. Gendiar, Prog. Theor. Phys. **105**, 409 (2001); A. Gendiar, N. Maeshima, and T. Nishino, Prog. Theor. Phys. **110**, 691 (2003).
- ⁵⁹ G. Vidal, Phys. Rev. Lett. **99**, 220405 (2007); **101**, 110501 (2008); L. Cincio, J. Dziarmaga, and M. M. Rams, *ibid.* **100**, 240603 (2008); G. Evenbly and G. Vidal, *ibid.* **102**, 180406 (2009); **112**, 240502 (2014); Phys. Rev. B **79**, 144108 (2009); **89**, 235113 (2014).